Time-Lapse Retinal Ganglion Cell Dendritic Field Degeneration Imaged in Organotypic Retinal Explant Culture

Thomas V. Johnson, Ericka N. Oglesby, Matthew R. Steinhart, Elizabeth Cone-Kimball, Joan Jefferys, and Harry A. Quigley

Glaucoma Center of Excellence, Wilmer Ophthalmological Institute, Johns Hopkins University School of Medicine, Baltimore, Maryland, United States

Correspondence: Thomas V. Johnson, Wilmer Eye Institute, Johns Hopkins Hospital, 600 North Wolfe Street, Wilmer B-29, Baltimore, MD 21287, USA; tvjohnson@jhmi.edu.

Submitted: July 22, 2015
Accepted: December 15, 2015

Citation: Johnson TV, Oglesby EN, Steinhart MR, Cone-Kimball E, Jefferys J, Quigley HA. Time-lapse retinal ganglion cell dendritic field degeneration imaged in organotypic retinal explant culture. *Invest Ophthalmol Vis Sci*. 2016;57:253–264. DOI:10.1167/iovs.15-17769

Purpose. To develop an ex vivo organotypic retinal explant culture system suitable for multiple time-point imaging of retinal ganglion cell (RGC) dendritic arbors over a period of 1 week, and capable of detecting dendrite neuroprotection conferred by experimental treatments.

Methods. Thy1-YFP mouse retinas were explanted and maintained in organotypic culture. Retinal ganglion cell dendritic arbors were imaged repeatedly using confocal laser scanning microscopy. Maximal projection z-stacks were traced by two masked investigators and dendritic fields were analyzed for characteristics including branch number, size, and complexity. One group of explants was treated with brain derived neurotrophic factor (BDNF) and ciliary neurotrophic factor (CNTF) added to the culture media. Changes in individual dendritic fields over time were detected using pair-wise comparison testing.

Results. Retinal ganglion cells in mouse retinal explant culture began to degenerate after 3 days with 52.4% surviving at 7 days. Dendritic field parameters showed minimal change over 8 hours in culture. Intra- and interobserver measurements of dendrite characteristics were strongly correlated (Spearman rank correlations consistently > 0.80). Statistically significant ($P < 0.001$) dendritic tree degeneration was detected following 7 days in culture including: 40% to 50% decreases in number of branch segments, number of junctions, number of terminal branches, and total branch length. Scholl analyses similarly demonstrated a significant decrease in dendritic field complexity. Treatment of explants with BDNF+CNTF significantly attenuated dendritic field degeneration.

Conclusions. Retinal explant culture of Thy1-YFP tissue provides a useful model for time-lapse imaging of RGC dendritic field degeneration over a course of several days, and is capable of detecting neuroprotective amelioration of dendritic pruning within individual RGCs.

Keywords: retinal ganglion cell, organotypic culture, dendrite, confocal imaging, neurodegeneration, glaucoma

The irreversible death of retinal ganglion cells (RGCs) is the central common end-point of all optic neuropathies, glaucoma being the most common. The cellular and molecular cascades implicated in glaucomatous RGC loss are extensive,[1] and elucidating the mechanisms by which RGCs die in glaucoma is requisite to the development of targeted treatment strategies aimed to prevent vision loss by increasing neuronal survival.[2–6] Moreover, reparative strategies aimed at improving vision through endogenous regeneration or cell transplantation must take into account the survival and functional status of residual host retinal architecture including the axons and dendrites of RGCs.[7,8] Compartmentalization of the RGC death process within cellular domains is being increasingly appreciated, though a complete understanding of the sequence of events leading from RGC injury to vision loss remains elusive. It is generally thought that the site of primary RGC injury in glaucoma is axonal and is associated with biomechanical deformation of the lamina cribrosa.[9–11] Eventually, this leads to anterograde and retrograde axonal degeneration, cellular apoptosis, and dendritic field loss with demise of the associated afferent and efferent neural synapses. Evidence suggests that these related processes hold some degree of molecular pathway independence and can be experimentally isolated, at least temporarily.[12–14] Such evidence is strongest for processes occurring in the axon and cell body. Dendritic and afferent synapse pruning has been documented in animal models of glaucoma[15] and imaging suggests that dendritic arbors shrink following insult, though the precise timing, patterns, and mechanisms of RGC dendrite degeneration in glaucoma are incompletely understood.

Evaluation of the RGC dendritic tree requires advanced imaging and analysis techniques capable of discriminating fine details of complex submicrometer fiber arrays. This poses several significant challenges, particularly in the rodent model systems most commonly employed to study glaucoma. In vivo imaging requires the presence of an RGC-specific label that actively traffics to or passively localizes within dendrites. While confocal laser scanning ophthalmoscopy techniques with and

without adaptive optics have generated an impressive ability to visualize RGC cellular structure in vivo over a period of days to months,[16–19] present technology has difficulty achieving the resolution necessary to discern fine detail. In vivo experimentation also poses difficulties related to local delivery of experimental compounds and precludes simultaneous electrophysiological recording. Ex vivo imaging techniques, which generally achieve higher resolution than in vivo imaging, have been developed and applied to healthy tissue, retinal tissue with prior RGC injury induced in vivo, and short term ex vivo physiological stress. However, so far these techniques have been limited to very short experiments (on the order of hours)[20] or single time-point analyses.[21–25] The significant degree of heterogeneity in the size, shape, and patterns of RGC dendritic fields therefore necessitate that a large of number of cells be analyzed in order to discriminate population-level mean differences in dendritic field characteristics between experimental groups imaged at single time points following injury. Further, classification of RGC subtype can be hampered by lack of information about the dendritic field at baseline, prior to injury.[26]

In order to address these limitations, we used organotypic culture of retinal tissue from mice genetically engineered to express an RGC-specific fluorescent tracer to facilitate dendritic field imaging ex vivo at high resolution using confocal microscopy. The pathogenesis of RGC injury in this model is primarily one of mechanical axonal trauma, and therefore more comparable to in vivo optic nerve crush or transection injury models than ocular hypertension induction, however the greater experimental tissue access afforded by tissue culture permits study at higher resolution than is possible in other systems. We employed previously described tissue culture techniques to maintain living explants for a period of up to 7 days, allowing time-lapse imaging of dendritic fields of the same RGC over time, which permitted within-cell paired statistical comparisons of dendritic field structure. A semiautomated system was used to trace dendritic trees prior to analysis, and a careful determination of intra- and interoperator variability in data acquisition was carried out. Analyses characterized potential dendritic field attenuation that was induced by the attendant axotomy involved in producing organotypic culture and demonstrated that these degenerative changes are ameliorated, in part, by treatment with neurotrophins.

Methods

Animals

Adult (10- to 16-week old) CD1 or Thy1-YFP (B6.Cg-Tg[Thy1-YFP]2Jrs/J strain; Jackson Laboratory, Bar Harbor, ME, USA) mice[27] were maintained in accordance with guidelines set forth by the ARVO Statement for the Use of Animals in Ophthalmic and Vision Research, using protocols approved and monitored by the Johns Hopkins University School of Medicine Animal Care and Use Committee (Baltimore, MD, USA).

Retinal Explant Culture

Primary retinal explants were isolated and organotypically cultured as previously described.[28–30] Briefly, mice were euthanized by intraperitoneal injection of ketamine (50 mg/kg, Fort Dodge Animal Health, Fort Dodge, IA, USA), xylazine (10 mg/kg; VedCo Inc., Saint Joseph, MO, USA), and acepromazine (2 mg/kg; Phoenix Pharmaceuticals, Burlingame, CA, USA). Globes were excised and the retinae were dissected free from RPE and cut radially into quarters such that each retinal explant represented one fourth of an entire retina. The neural retina was then flat-mounted with the photoreceptor side down against a polytetrafluoroethylene membrane (EMD Millipore, Billerica, MD, USA) at an air-fluid interface overlying culture media composed of Neurobasal-A media with B27 supplement (2%), N2 supplement (1%), L-glutamine (0.8 mM), penicillin (50 IU/mL), and streptomycin (50 μg/mL) in humidified conditions at 37°C and 5% CO_2. Half of the culture media was exchanged every 2 to 4 days.

In some experiments, culture media was supplemented with forskolin (20 μg/mL; Sigma-Aldrich Corp., St. Louis, MO, USA) + brain derived neurotrophic factor (BDNF, 50 ng/mL; Sigma-Aldrich Corp.) + ciliary neurotrophic factor (CNTF, 50 ng/mL; Sigma-Aldrich Corp.) or with forskolin only as a negative control. A 2-μL droplet of complete media was placed on the RGC surface of retinal explants every 2 to 4 days to ensure adequate exposure to trophic supplements.

Histology and Histologic Analysis

Retinal explants derived from CD1 mice were fixed at various time points by immersion in cold 4% paraformaldehyde for 24 hours. Flat-mounted retinal explants were processed for immunofluorescent analysis at room temperature by washing twice in PBS, simultaneously permeabilizing and blocking using a solution of Triton X-100 (0.1%) and normal goat serum (5%) in PBS for 90 minutes, incubating with primary antibody (anti–β-III-Tubulin [Tuj1]; Neuromics, Edina, MN, USA) in blocking solution overnight, and incubating with secondary antibody (Alexa Fluor-488 goat anti-chicken IgG; Thermo Fisher Scientific, Grand Island, NY, USA) in blocking solution for 3 hours. 4′,6-diamidino-2-phenylindole (DAPI) was included in the penultimate wash to facilitate visualization of nuclei.

Flat-mounted retinal explants were imaged in a single plane centered through the RGC layer using a Zeiss 510 confocal microscope equipped with a ×20 objective (Carl Zeiss Microscopy, Thornwood, NY, USA). Five images were acquired per retinal explant at progressive eccentricities from the optic nerve head through the midline of the explanted tissue. $DAPI^+$ cells and β-III-$Tubulin^+$ RGCs were quantified in each micrograph by an investigator masked to the time point at which the tissue was fixed. Pynknotic or karyorrhexic nuclei detected with DAPI staining were excluded from the quantification of living cells. Data was averaged for each explant and linearly transformed to yield mean cell density in cells per millimeter squared.

Live Confocal Imaging

Live retinal explant cultures derived from Thy1-YFP mice were imaged at multiple time points using a Zeiss 710 confocal microscope equipped with a ×20 long-working distance objective and an environmental chamber set to a temperature of 37°C and ambient CO_2 (Carl Zeiss Microscopy). Cultures were removed from the incubator individually and placed in a petri dish containing complete culture medium but excluding phenol red, which was found to contribute background autofluorescence in preliminary experiments. Retinal ganglion cells were identified by YFP immunofluorescence and confirmed by the presence of an axon leading to the optic nerve head. An approximate map of RGC location was drawn for each retinal explant to facilitate relocalization of individual cells at later time points. Z-stacks were then acquired for four to seven RGCs per retinal explant using the following acquisition parameters: wavelength = 514 nm; laser intensity = 1.500%; pinhole = 1 AU; acquisition speed = 9; frame average = 4; image density = 8 bit; digital gain = 1.5; master gain =

variable (700–1200). Master gain was the only parameter that was adjusted between individual RGCs (but always kept constant within single RGCs at multiple time points), in order to optimize the signal for dendritic field visualization. Step size was limited such that stacks contained a maximum of 24 steps in order to limit potentially phototoxic laser exposure per cell. The number of RGCs imaged per retinal explant was similarly limited such that total time for each explant outside of the culture incubator was 30 minutes or less. Retinal ganglion cells were selected for imaging based on brightness and nonoverlap with adjacent RGCs. All RGCs within a single experiment were imaged in parallel at a single imaging session.

In some experiments, separate single-plane images of the cell soma were obtained through the plane with the greatest soma diameter. Wavelength, laser intensity, pinhole, acquisition speed, frame average, image density, and digital gain were as above. Master gain was varied on an individual RGC basis at the day 0 time point in order to obtain an image through the center of the soma with the greatest signal intensity where no more than 2 to 3 pixels were saturated, according to the saturation heat map imaging mode in the Zen image acquisition software. Retinal ganglion cells were reimaged at the day 7 time point using the specific master gain setting that was used for that particular RGC at day 0.

Dendritic Field Analysis

Retinal ganglion cell z-stacks were used to create two dimensional maximum projection images using Zen software (v2012; Carl Zeiss). Maximum projection images were then traced to create RGC skeletons in a semiautomated fashion by two independent investigators who were masked to cell identity using the NeuronJ plugin[31] (in the public domain, http://www.imagescience.org/meijering/software/neuronj/) for ImageJ software (http://imagej.nih.gov/ij/; provided in the public domain by the National Institutes of Health, Bethesda, MD, USA). Axons were excluded from the tracings. Retinal ganglion cell dendritic field skeletons were analyzed using Fiji[32] (in the public domain, http://fiji.sc/Fiji), which measured: number of branch segments (dendrite segments between branch points, crossings, or terminations); number of junctions (branch points and crossings); terminal branches; average branch length, maximum branch length, and total branch length (number of branch segments × average branch length). Sholl analyses were also performed on RGC dendritic field skeletons using Fiji. Sholl rings were centered at the midpoint of the long axis of the cell body and spaced at 5-μm intervals beginning 10 μm from the center. Measurements included area under the curve (AUC) of the Scholl Histogram, number of dendritic field intersections per Sholl ring, total number of intersections per RGC, average number of intersections per Scholl ring, maximal number of intersections per RGC, and enclosing radius (the most distant Sholl ring that intersected the dendritic tree).

Cell Soma YFP Signal Intensity Analysis

Single-plane images acquired through the cell soma were analyzed to determine average YFP signal intensity using ImageJ. The perimeter of each cell soma was hand traced by an investigator masked to RGC identity and minimal, maximal, and average channel intensity within the soma were measured.

Statistical Analyses

Analyses of RGC loss in wild-type CD1 explants were carried out by determining the mean cell density per explant and averaging for each time point. Changes in cell density over time were determined by one-way ANOVA followed by Dunnett's post hoc test comparing each time point to the day 0 time point. Analyses of dendritic field parameters were carried out by comparing data from single RGCs obtained at different time points using 2-tailed paired Student's *t*-tests and by comparing dendritic field parameters or change in field parameters in separate groups of RGCs (i.e., skeletons traced by different investigators or explants cultured under different treatment conditions) using 2-tailed unpaired Student's *t*-tests for parametric data sets or using Wilcoxon rank sum tests for nonparametric data sets. Spearman rank correlations were used to assess interobserver reliability by comparing data obtained from single RGCs traced by different investigators and were used to assess intraobserver reliability by comparing data from individual RGCs imaged twice less than 8 hours apart and traced by the same investigator, respectively. In all figures, error bars represent SD for data describing mean values of dendritic field parameters at single time points, and they represent SEM for data describing percent change in dendritic field parameters over periods of time.

Results

Characterization of RGC Loss in Mouse Retinal Explants

Prior work in rat retina has shown that organotypic culture causes slow, progressive degeneration of RGCs over the course of 3 to 14 days ex vivo.[28,29] To determine the time course of RGC degeneration in mouse retinal explants cultured under similar conditions, retina from wild-type CD1 mice were explanted and cultured for 0, 1, 3, 7, 10, or 14 days prior to fixation ($N = 5$ retinal explants per time point) and subsequent immunofluorescent labeling of all cells ($DAPI^+$) or RGCs (β-III-$Tubulin^+$). Representative micrographs are shown in Figure 1A through 1F. Analyses demonstrated that in healthy mouse retina, RGCs comprise approximately 50% of the RGC layer cells, with the remainder presumably being displaced amacrine cells, microglia, and astrocytes. The number of RGCs remained relatively constant for the first 3 days in culture, declining steadily thereafter (Figs. 1G, 1H) with a statistically significant ($P < 0.001$, Dunnet's test) loss of RGCs evident by day 7 compared with day 0. The non-RGC population, in contrast, remained relatively constant through 14 days of culture, suggesting that within the RGC layer, the retinal explant culture model is a relatively specific trigger for RGC degeneration through day 14, similar to the effect of optic nerve transection in vivo.[33]

Characterization of RGC Dendritic Fields

Thy1-YFP^+RGC dendritic fields were first analyzed immediately following explantation to determine the feasibility of obtaining reliable and reproducible data from confocal imaging of live tissue. A sample of 16 RGCs from four retinal explants of one mouse were imaged twice, 8 hours apart, and two investigators independently traced skeletons based on the z-stack maximum projections. Representative RGC maximum projections with corresponding skeleton tracings are shown in Figure 2A through 2F. Qualitatively, little to no difference in the morphology of the dendritic tree was observable between the two time points. Quantitative analyses of RGC dendritic field parameters confirmed a lack of statistical change in dendritic tree morphology over 8 hours in culture and showed good inter- and intraobserver consistency (Figs. 2G–L, $P > 0.05$ for all comparisons by Wilcoxon rank sum tests). While small interobserver differences in data obtained from the same RGCs

Investigative Ophthalmology & Visual Science

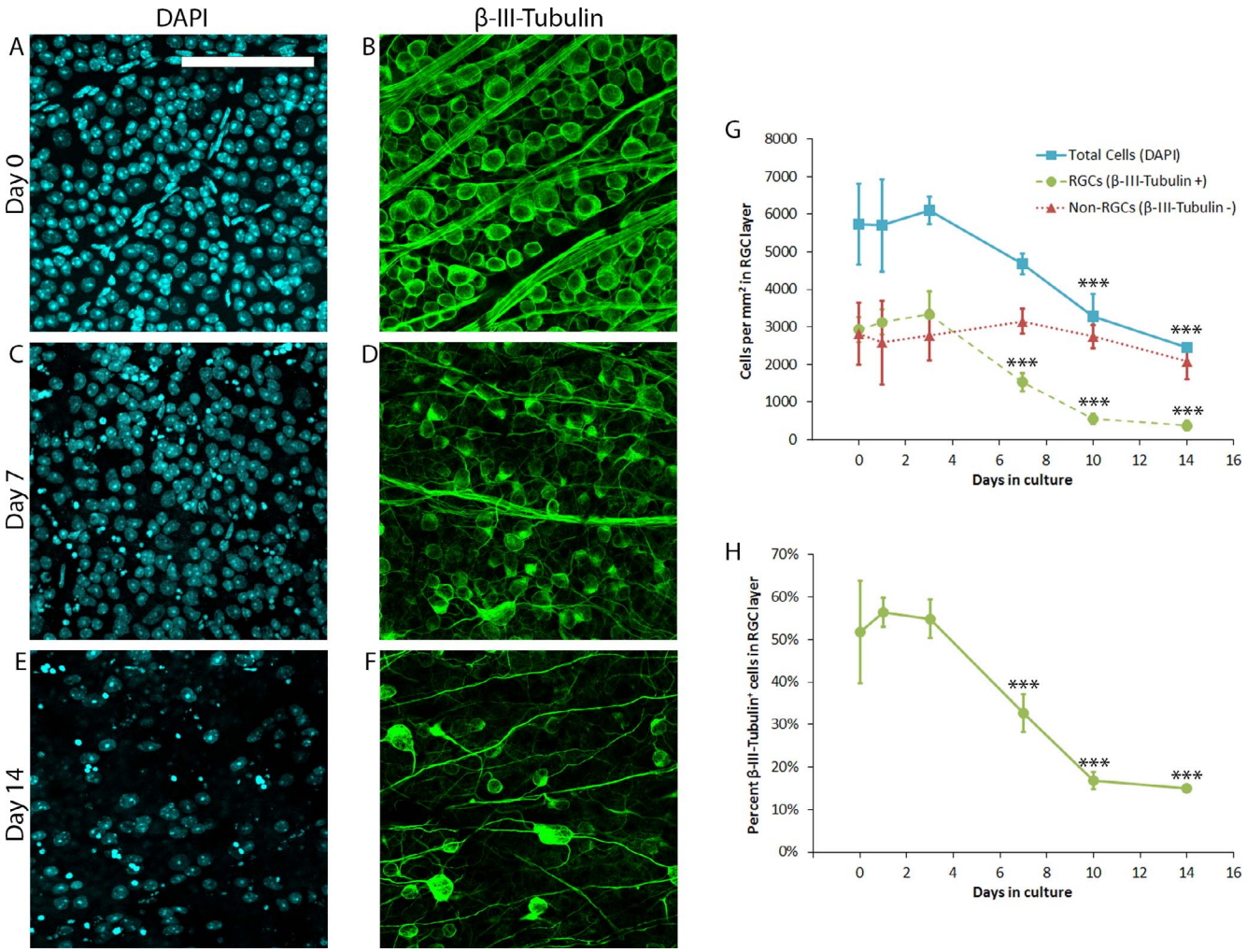

Figure 1. Characterization of RGC loss in mouse retinal explants. Wild-type CD1 mouse retinal explants ($N = 5$ explants per time point) were cultured for 0, 1, 3, 7, 10, or 14 days prior to fixation and immunofluorescent labeling of all cells (DAPI$^+$, [**A**, **C**, **E**]) or RGCs (β-III-Tubulin$^+$, [**B**, **D**, **F**]). Representative micrographs from nonoverlapping fields are shown in (**A–F**); *scale bars*: 100 μm. Quantification of DAPI$^+$ and β-III-Tubulin$^+$ cell density is presented in G. Non-RGCs represent the difference between DAPI$^+$ and β-III-Tubulin$^+$ cells. Percent β-III-Tubulin$^+$ cells in the RGC layer is presented in (**H**). *Error bars* represent SD. $^{***}P \leq 0.001$ by Dunnett's post hoc test compared with day 0 time point.

existed, interobserver Spearman rank correlations (ρ) at the 0 hour time point all exceeded 0.80: # branches, $\rho = 0.91$; # junctions, $\rho = 0.88$; # terminal branches, $\rho = 0.91$; average branch length, $\rho = 0.94$; maximum branch length, $\rho = 0.84$; total branch length, $\rho = 0.99$. Comparable interobserver ρ values were obtained at the 8h time point: # branches, $\rho = 0.90$; # junctions, $\rho = 0.83$; # terminal branches, $\rho = 0.95$; average branch length, $\rho = 0.97$; maximum branch length, $\rho = 0.91$; total branch length, $\rho = 0.98$. Intraobserver skeletons for individual RGCs analyzed at 0 and 8 hours showed parameter variability of no more than 5% (Fig. 2M) with a relatively low variance in the percent change over 8 hours for any parameter (Fig. 2N). Intraobserver Spearman rank correlations were uniformly greater than or equal to 0.88 for all parameters between the two time points for both investigators, suggesting that RGC dendritic trees underwent essentially no change in the first 8 hours of culture and that the image acquisition, tracing, and analysis methods employed were highly reproducible. Sholl histograms and field parameters for RGCs imaged at 0 and 8 hours and traced by investigator #1 similarly demonstrated minimal change (Figs. 2O–S). The peak number of Scholl intersections occurred, on average, at approximately 60 to 70 μm from center of the soma.

RGC Dendritic Field Changes Over 7 Days in Culture

Given the reliability and reproducibility of the RGC dendritic field analysis method developed for living cells, RGCs were imaged immediately after explantation and at a longer interval of 7 days to establish the natural course of dendritic field degeneration in the retinal explant culture model. A total of 75 RGCs from 21 retinal explants of three mice were imaged. There was a range of dendritic field changes observed for individual RGCs, with some RGCs exhibiting minimal change (Figs. 3A, 3B), some exhibiting moderate dendritic degeneration (Figs. 3C, 3D, changes in dendritic field parameters for this cell approximated the average changes for the group), and some exhibiting severe dendrite degeneration (Figs. 3E, 3F). Qualitatively, dendrite branches became less smooth over the course of 7 days in culture, with development of blebs, outpouchings, beading, and fragmentation, especially at greater distances from the soma. No significant evidence of neurite sprouting, reactive plasticity, or migration was observed on a structural basis, though molecular analyses were not undertaken. Dendritic field parameters were analyzed using skeletons traced by both investigators (Figs. 3G–M).

Investigative Ophthalmology & Visual Science

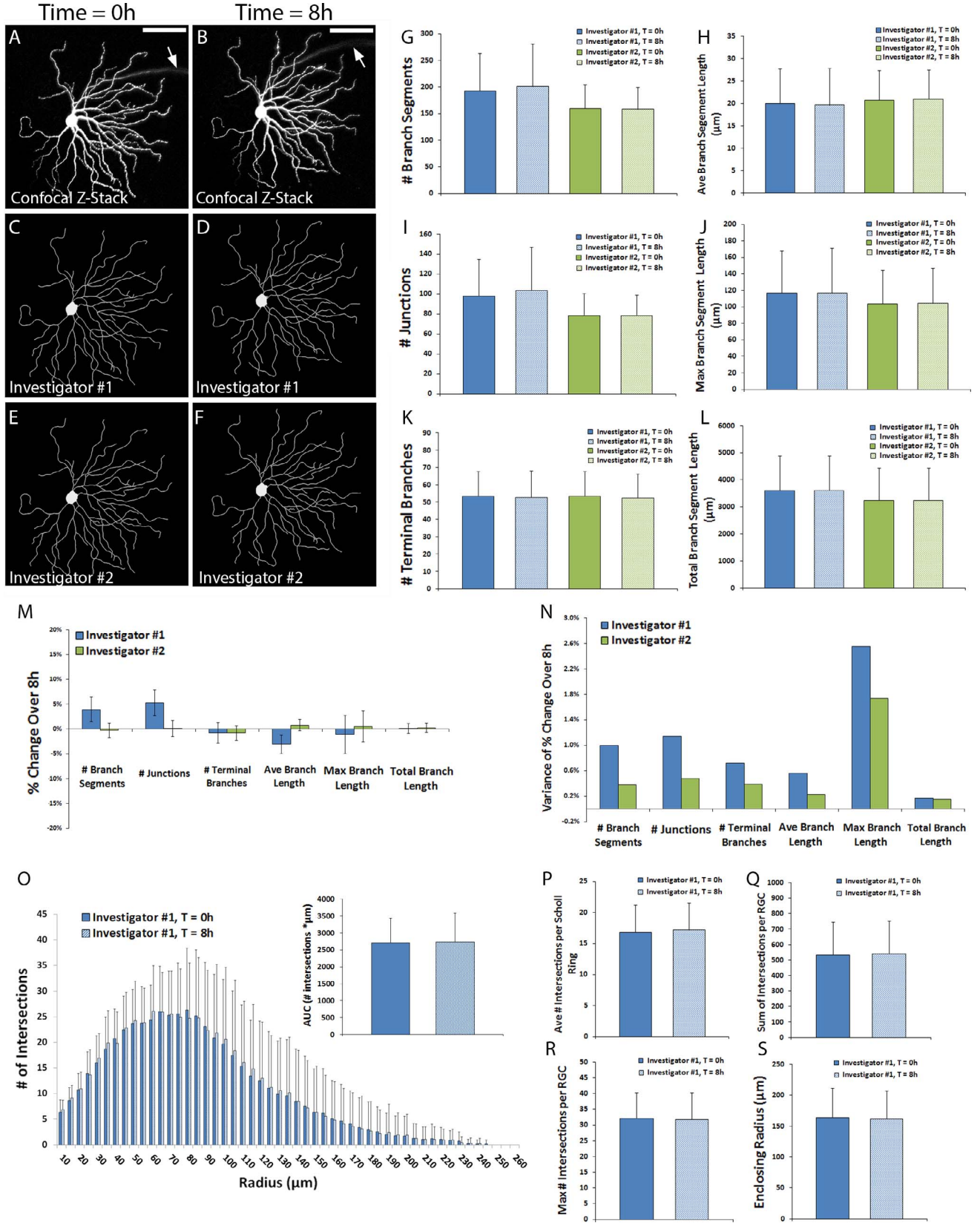

Figure 2. Characterization of RGC dendritic fields at 0 and 8 hours of culture. Thy1-YFP retinal explants were cultured for 7 days. Z-stack confocal images of live YFP$^+$ RGCs ($N = 16$ RGCs) were obtained on day 0 and day 7. Two investigators masked to RGC identity traced the dendritic field of each RGC. Representative micrographs of z-stack maximum projections (**A**, **B**) and investigator skeleton tracings (**C**–**F**) are shown; *scale bars*: 100 µm; *arrow* points to the axon, which was excluded from the tracing. Dendritic field parameters (**G**–**L**), changes in field parameters over 8 hours (**M**), and variance of change in field parameters (**N**) are shown. Scholl histograms (**O**) depict the number of intersections between dendritic fields and Sholl rings of increasing eccentricity; *inset graph* quantifies the AUC of the Scholl histogram. Sholl parameters are shown (**P**–**S**). *Error bars* in (**G**–**L**) and (**O**–**S**) represent SD; *error bars* in (**M**) represent standard error of the mean. $P > 0.05$ by Wilcoxon Sum Rank tests for all comparisons.

Investigative Ophthalmology & Visual Science

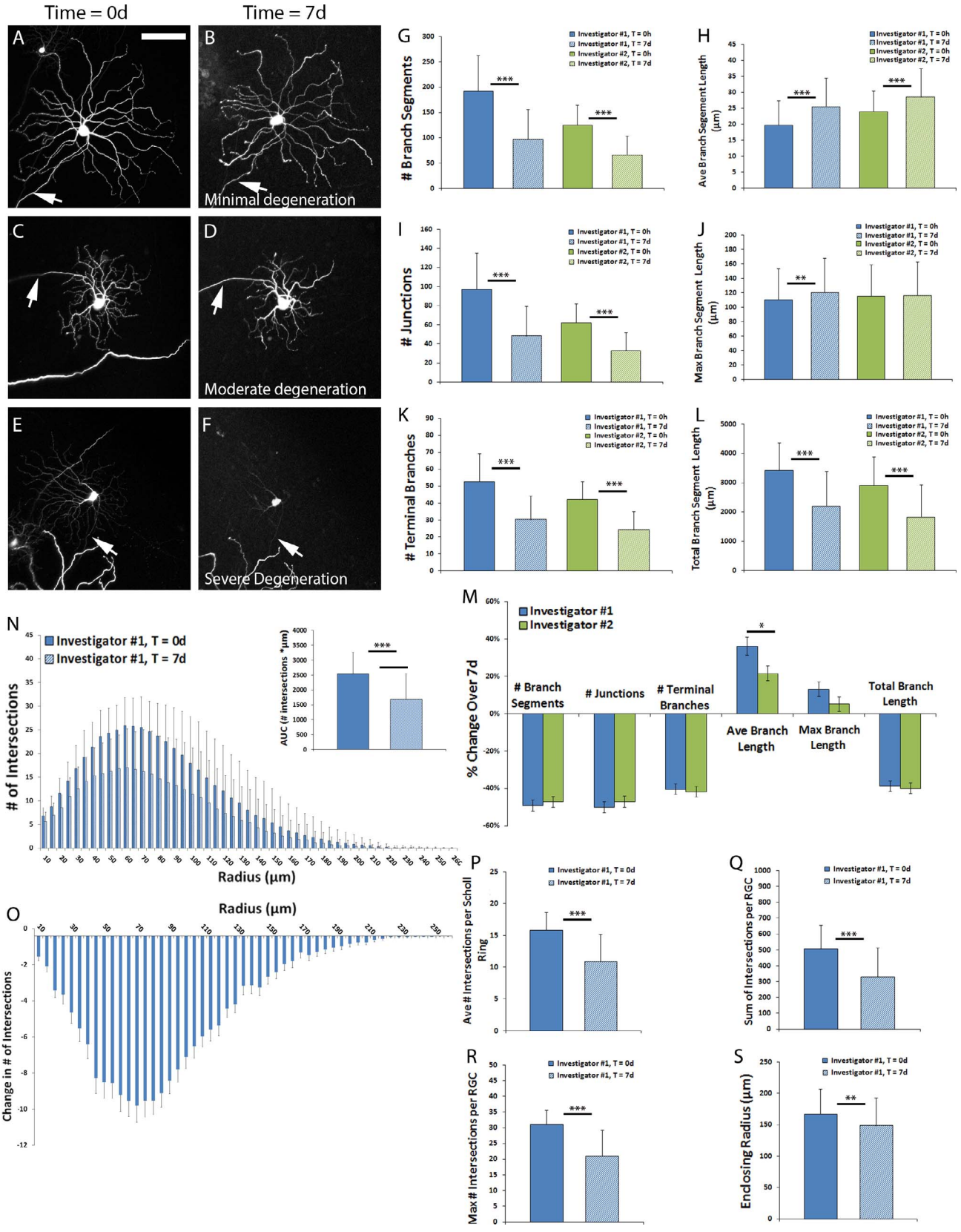

Figure 3. Retinal ganglion cell dendritic field changes over 7 days in culture. Thy1-YFP retinal explants were cultured for 7 days. Z-stack confocal images of live YFP$^+$ RGCs ($N = 75$ RGCs) were obtained on day 0 and day 7. Two investigators masked to RGC identity traced the dendritic field of each RGC. Representative micrographs of z-stack maximum projections showing RGCs with minimal (**A**, **B**), moderate (**C**, **D**), and severe (**E**, **F**) levels of dendritic field degeneration over 7 days are shown; *scale bar* represents 100 µm; *arrow* points to the axon, which was excluded from the tracing. Dendritic field parameters (**G**–**L**) and changes in field parameters over 8 hours (**M**) are shown. Scholl histograms (**N**) depict the number of intersections between dendritic fields and Sholl rings of increasing eccentricity; *inset graph* quantifies the AUC of the Scholl histogram. The average

Investigative Ophthalmology & Visual Science

change in Sholl histogram over 7 days (**O**) and Sholl parameters at both time points are shown (**P–S**). *Error bars* in (**G–L**, **N**, **P–S**) represent SD; *error bars* in (**M**, **O**) represent SEM. $^{**}P \leq 0.01$ and $^{***}P \leq 0.001$ by paired *t*-test comparing individual RGCs at both time points. $^{*}P \leq 0.05$ by paired *t*-test comparing change in field parameter between investigator tracings.

Significant ($P < 0.001$, paired *t*-test) decreases of between 40% and 50% in number of branches (Fig. 3G), number of junctions (Fig. 3I), number of terminal branches (Fig. 3K), and total branch length were identified (Fig. 3L), while average branch length significantly increased (Fig. 3H), likely mediated by loss of shorter dendritic branches. Maximum branch length increased modestly ($P < 0.01$, paired *t*-test), only in skeletons traced by investigator #1 (Fig. 3J). Of note, there was strong interobserver agreement regarding the percent change in each dendritic field parameter; investigator #1 found a significantly ($P < 0.05$, paired *t*-test) greater increase in average branch length compared with investigator #2 (Fig. 3M).

Sholl histograms demonstrated a consistent eccentricity of peak intersections at both time points, approximately 60 μm from the center of the soma (Fig. 3N). The number of intersections overall decreased significantly after 7 days in culture, in a pattern that mirrored the baseline density of intersections (Fig. 3O). The AUC of the Scholl Histogram decreased significantly ($P < 0.001$, paired *t*-test) following 7 days in culture. The average (Fig. 3P), sum (Fig. 3Q), and maximal number of intersections (Fig. 3R) all decreased significantly ($P < 0.001$, paired *t*-test) by approximately 30% while the enclosing radius decreased significantly ($P < 0.01$, paired *t*-test) by only 6.7% (Fig. 3S).

A subset of RGCs that were imaged at day 0 completely degenerated and these were not present to be imaged at day 7. Given that more than one-third of RGCs are lost by day 7 of culture by tubulin labeling (Fig. 1G), it was expected that only a portion of fluorescent RGCs imaged at day 0 would still be alive in culture at day 7. To determine whether there were any baseline morphologic characteristics that could distinguish RGCs more likely to die early in culture (and therefore lead to possible sampling bias), the day 0 dendritic field parameters of RGCs imaged at day 0 and at day 7 ($N = 75$, as above) were compared with the baseline day 0 dendritic field parameters of RGCs imaged at day 0 but no longer alive in culture at day 7 ($N = 55$). Analyses demonstrated no significant baseline differences ($P > 0.05$, unpaired *t*-test) in any dendritic field parameter or Sholl parameter between these two groups of cells (Figs. 4A–K), so there is no evidence that they correlate with any particular RGC subclass described in previous literature.

Amelioration of RGC Dendritic Field Changes Over 7 Days by BDNF+CNTF

After establishing the pattern of RGC dendritic field degeneration in cultured retinal explants over 7 days, the effects of trophic factor supplementation on this process were evaluated. Retinal explants were either cultured as previously described with the addition of forskolin, which on its own does not confer direct neuroprotective effects but which potentiates the activity of neurotrophins ($N = 74$ RGCs), or with the addition of BDNF+CNTF+forskolin ($N = 48$ RGCs). Dendritic field analyses demonstrated a modest, but statistically significant ($P < 0.05$, unpaired *t*-test) baseline difference in the number of branches (Fig. 5A), junctions (Fig. 5C), and terminal branches (Fig. 5E), but not average (Fig. 5B), maximum (Fig. 5D), or total branch length (Fig. 5F) for these two groups. After 7 days in culture, significant ($P < 0.001$, paired *t*-test) decreases in number of branches (Fig. 5A), junctions (Fig. 5C), terminal branches (Fig. 5E), and total branch length (Fig. 5F) were noted within both groups, while significant increases in average (Fig. 5B) and maximum (Fig. 5D) branch length also were found. The extent of branch, junction, terminal branch, and total branch length decrease was significantly lower ($P < 0.01$ for all comparisons, unpaired *t*-test) in the BDNF+CNTF group as compared with the control group (Fig. 5G).

Sholl analyses also demonstrated significantly reduced dendritic loss in the BDNF+CNTF+forskolin group compared with forskolin only ($P < 0.01$, unpaired *t*-test comparing AUC of change in Scholl histogram, Figs. 5H, 5I). In addition, the BDNF+CNTF+forskolin group demonstrated a significantly ($P < 0.05$, unpaired *t*-test) greater number of total (Figs. 5L, 5O) and maximal Sholl intersections (Figs. 5M, 5O), while the difference in the loss of average Sholl intersections did not meet statistical significance (Figs. 5K, 5O, $P = 0.06$, unpaired *t*-test). Enclosing radius was not different between groups or time points (Figs. 5N, 5O).

In order to determine the likelihood that variability or attenuation of YFP signal intensity may have limited visualization of the dendritic tree in full or otherwise contributed to the differences observed when retinal explants were treated with BDNF+CNTF+forskolin, the YFP signal intensity was measured in a standardized fashion in the cell bodies of RGCs from both groups. Analyses demonstrated that signal intensity decreased in both groups: Forskolin only = 145 ± 21 units at baseline compared with 58 ± 41 units at 7 days; BDNF+CNTF+forskolin 143 ± 16 units at baseline compared with 66 ± 45 units at 7 days ($P < 0.001$ for both comparisons). The difference between the average decrease in YFP signal intensity of 59 ± 28% in the forskolin only group and 55 ± 30% in the BNDF+CNTF+forskolin group was not statistically significant ($P > 0.05$, unpaired *t*-test).

Discussion

Characterizing the molecular processes underlying RGC degeneration is central to understanding and developing treatments for optic neuropathies including glaucoma. Prior to RGC death, functional and structural changes occur, including retraction and remodeling of dendritic arbors altering receptive field characteristics and ultimately visual perception. Studies aimed at detecting changes in the dendritic arbors of injured RGCs are shedding light on this process, but experimental limitations of various model systems exist. The present work demonstrates that individual, living RGCs and their dendritic arbors can be imaged at high resolution in situ over several days. While prior work has imaged structures as detailed as dendritic spines in living cultured RGCs over a period of hours,[20] this study represents, to our knowledge, the first report of time-lapse ex vivo RGC dendritic arbor imaging over a period of 1 week.

We used a previously well-characterized organotypic culture model wherein RGC cell bodies survive for at least 2 weeks in culture,[28] using tissue from Thy1-YFP mice, which have been widely used for the purposes of RGC dendritic field imaging.[17–19,21,22,24,25] This confirmed the feasibility and reliability of high-resolution imaging of living cultured RGCs and analysis of dendritic field characteristics. We identified no acute changes to RGC dendrites that were evident within a period of 8 hours following axotomy, explantation, and a single imaging session, but there was a statistically significant decrease in the number of branch segments, terminal branches, junctions, total branch length, and Scholl complexity after 1 week in culture. The increase in average branch length

Investigative Ophthalmology & Visual Science

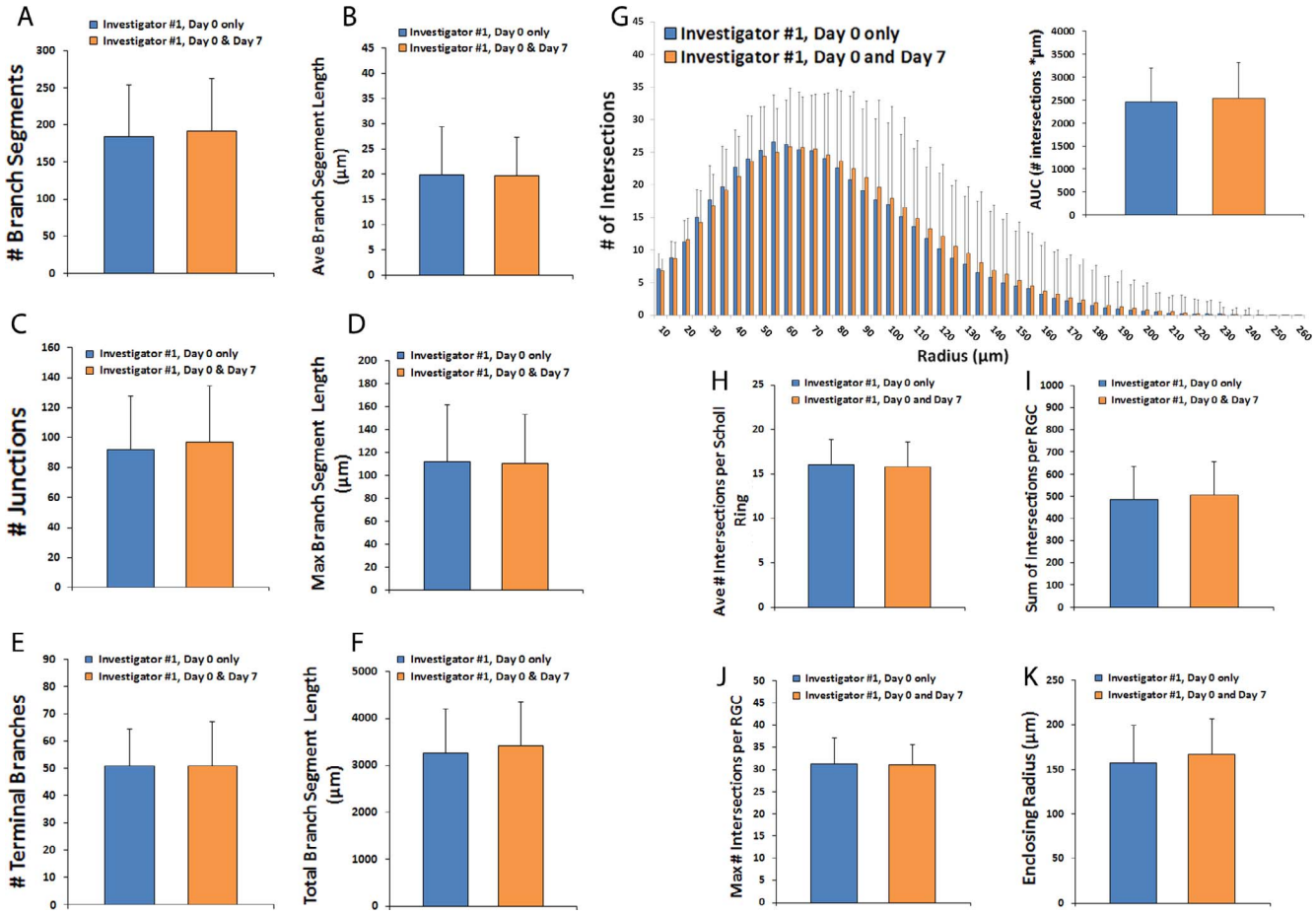

Figure 4. Comparison of dendritic fields in RGCs living versus dead after 7 days in culture. Thy1-YFP retinal explants were cultured for 7 days. Z-stack confocal images of live YFP$^+$ RGCs ($N = 130$ RGCs) were obtained on day 0 only and cells were divided according to whether they were still alive and visible by microscopy at 7 days ($N = 75$ RGCs) or were no longer detectable at 7 days ($N = 55$ RGCs). Dendritic field parameters (**A–F**) for RGCs imaged at day 0 are shown. Scholl histograms (**G**) depict the number of intersections between dendritic fields and Sholl rings of increasing eccentricity; *inset graph* quantifies the AUC of the Scholl histogram. Sholl parameters for day 0 images are shown (**H–K**). *Error bars* represent SD. $P > 0.05$ by unpaired *t*-test for all comparisons.

was likely mediated by loss of shorter dendritic branches, as shown previously following optic nerve crush in vivo,[17,22] which attests to the value of this system in modeling clinical optic nerve injury and degeneration. While a subset of RGCs was completely lost by the 7 day time point in explant culture, there was no baseline morphologic dendritic tree parameter that differentiated the group of RGCs that survived to 7 days from that which had died. While this is in contrast to an in vivo optic nerve axotomy model where alpha-RGCs were found to both survive and regenerate axons at significantly higher rates than other RGC subclasses,[34] the present study limited RGC class discrimination to measures of transverse dendritic field morphology. More nuanced immunohistochemical or transgenic methods of identifying specific RGC subclasses could be utilized to determine if dendritic tree degeneration is class-specific in the present model.

Importantly, a statistically significant protective effect of BDNF+CNTF treatment on the dendritic trees of RGCs was identified. In addition, BDNF has been shown previously to enhance RGC soma survival in this model.[29] These findings lend additional validity to explant culture serving as a model for in vivo RGC degeneration, as BNDF also improves RGC survival and protects dendritic architecture following optic nerve injury.[35] CNTF treatment has been suggested to promote RGC dendrite regeneration, albeit with abnormal morphology,[36] and an effect that is dramatically increased when SOCS3 and/or Klf4 are deleted.[37,38]

A significant amount of work detailing the effects of various RGC insults on the dendritic tree in vivo and ex vivo has been published, and a comprehensive review of the data is beyond the scope of this discussion. However, several studies demonstrate particular benefits and limitations of various glaucoma modeling strategies and RGC imaging modalities that are worth discussion.

One critical factor necessary for RGC dendritic field imaging is a cell-specific compartmentalized marker. We recently used the Thy1-YFP mouse to analyze RGC dendrites following optic nerve crush and microbead-induced ocular hypertensive glaucoma.[22] However, the Thy1-YFP model has been criticized when used to investigate the effects of RGC stress and injury, as Thy1 itself may be downregulated in states of cell stress or in early stages of death.[39,40] Recent evidence suggested that Thy1-YFP labeling of RGCs may select for "healthier" RGCs with fewer signs of degeneration, at least in the DBA/2J mouse model, as compared with dye-based cell membrane labels.[25] This may explain why dendritic tree degeneration was not observed in Thy1-YFP animals with ocular hypertension induced by anterior chamber angle microbead occlusion.[22]

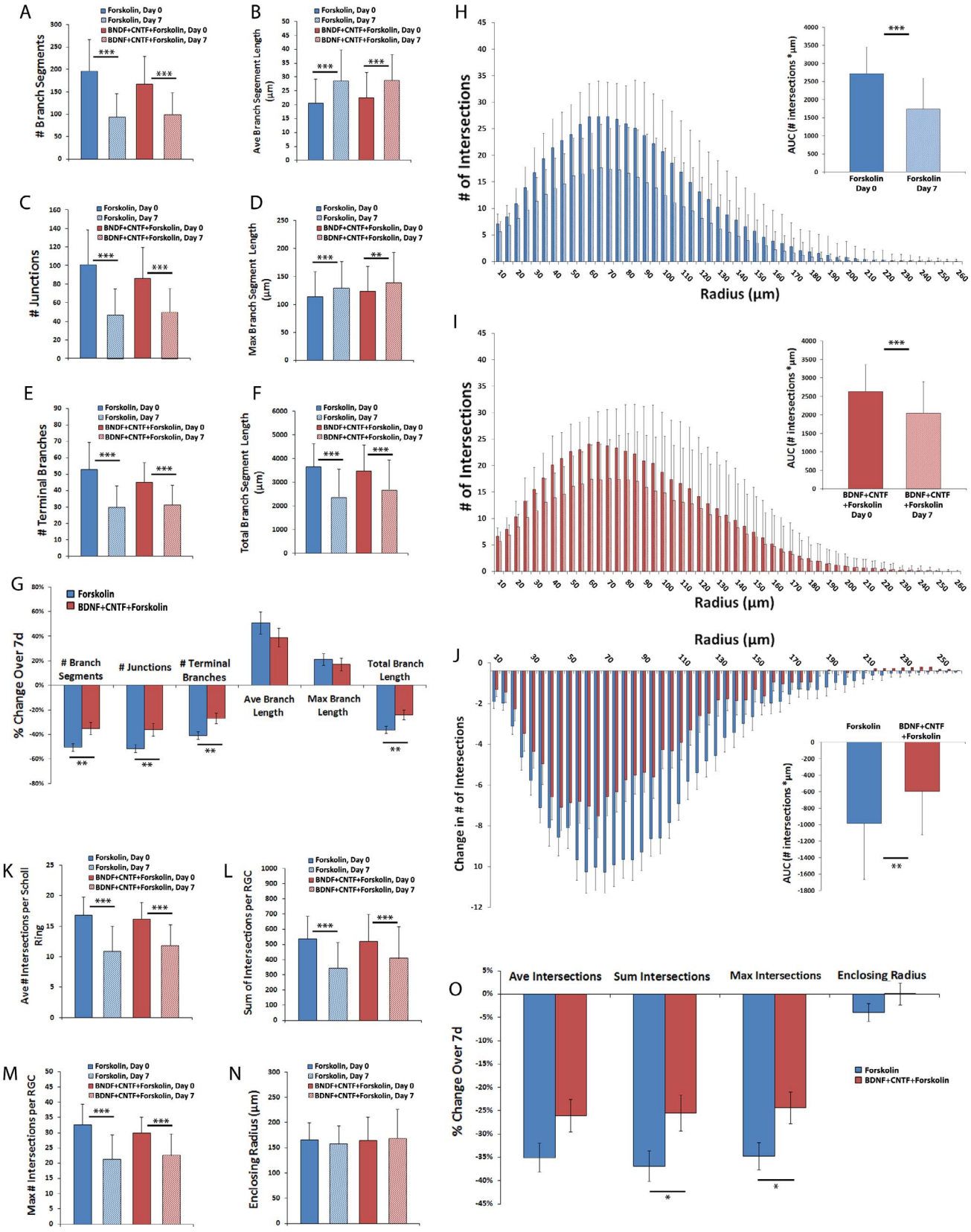

Figure 5. Amelioration of RGC dendritic field changes over 7 days by BDNF+CNTF. Thy1-YFP retinal explants were cultured for 7 days with forskolin (20 µg/mL)+BDNF (50 ng/mL)+CNTF (50 ng/mL; $N = 74$ RGCs) or with forskolin only as a negative control ($N = 48$ RGCs). Z-stack confocal images of live YFP$^+$ RGCs were obtained on day 0 and day 7. Dendritic field parameters (**A–F**) and changes in field parameters over 8 hours (**G**) are shown. Scholl histograms (**H–I**) depict the number of intersections between dendritic fields and Sholl rings of increasing eccentricity; *inset graph* quantifies the AUC of the Scholl histogram. Sholl parameters at both time points, (**K–N**), and change in Sholl parameters over 7 days (**J**, **O**) are shown. *Error bars* in (**A–F**, **H–I**, **K–N**) represent SD; *error bars* in (**G**, **J**, **O**) represent SEM. (**A–F**, **K–N**, **H**, **I**): $^{**}P \leq 0.01$ and $^{***}P \leq 0.001$ by paired *t*-test comparing individual RGCs at both time points. (**G**, **J**, **O**): $^{*}P \leq 0.05$, $^{**}P \leq 0.01$ by unpaired *t*-test comparing change in field parameter between treatment groups.

Investigative Ophthalmology & Visual Science

That said, even following optic nerve crush, YFP signals that remain present overlap completely with immunofluorescent labeling of dendritic markers such as phosphorylated neurofilament,[17,19] suggesting that this issue is less likely to affect the valid delineation of individual dendritic trees that retain fluorescence. Thus, this seems to be a more pertinent issue for experimental models aimed at evaluating changes in RGC populations rather than in individual cells, where the change in YFP signal intensity for each cell type can be determined and serve as an internal control.

Intracellular application of dye is an alternative technique for labeling of RGCs prior to imaging, but requires enucleation and retinal explantation. Injection of dye using a microelectrode or patch pipette provides a highly targeted method for RGC imaging, and if combined with alternate methods of RGC subtype-specific labeling, allows for significant investigator control and efficiency.[41] This method is, however, time consuming and requires significant technical expertise. Particle-mediated ballistic delivery of fluorescent dyes (gene gun) is another method that has been used to label RGCs for dendrite analysis.[25,42] This method, however, could at least theoretically generate selection bias in cell labeling as cells with a larger soma would more likely be inoculated with particle. Both of these methods likely affect the long-term viability of the cell and, if followed over time, may themselves introduce changes to cell physiology and structure beyond the injury model being investigated.

One major limitation of most RGC imaging models is that imaging is limited to a single time point following injury. Because the dendritic trees of individual RGCs and RGC subclasses are diverse, large populations of cells must be imaged in order for early or subtle changes to dendrites to become detectable. Moreover, subclass specific effects of pathological processes may be hampered by misclassification of RGCs when only a postinjury image is used, because pruning of dendritic arbors from one subclass may actually resemble full dendritic arbors of another. Attempts have been made to reclassify RGC subgroups based on specific characteristics of the dendritic tree that are relatively stable during early stages of cell death with a success rate of between 60% and 75%, in a group of healthy, uninjured RGCs.[26] The present system provides a platform that could be used for subclassification based on morphology at the time of explantation prior to degenerative changes to the dendritic tree. While this limits experimental protocols to RGC insults that are introduced ex vivo, it eliminates uncertainty about the baseline morphology of the cells being studied. Moreover, it provides for more robust statistical analyses of changes in dendritic tree morphology over time, as single-cell, paired, repeat-measure testing rather than population level means testing can be employed.

An added benefit to imaging live RGCs involves the avoidance of fixation-induced artifact that may be especially relevant to RGC dendritic field analyses.[43] Formaldehyde-based fixation triggers the formation of varicosities within RGC axons and dendrites, which are not present in freshly imaged tissue but appear within a matter of minutes of fixation. Indeed, such swellings are readily visible in an array of published images of RGC dendritic fields analyzed postmortem.[18,22,24,25] Imaging of live cultured tissue, in contrast, avoids fixation altogether. Therefore, the morphologic changes described during the process of RGC degeneration (beading, blebbing, and fragmentation) are not attributable to fixation artifact.

Longitudinal time-lapse imaging of RGCs in vivo has been useful in following certain aspects of RGC structure over time following injury. Lindsey et al.,[17] evaluated the effects of systemic brimonidine treatment on RGC dendritic arbors as imaged in longitudinal fashion in vivo in Thy1-YFP transgenic mice following optic nerve crush. Impressively, a significant subset of RGCs imaged was amenable to Scholl analysis similar to that presented in the current work. Nonetheless, it is unclear whether the resolution of images obtained using this system truly obtained all structural information that would have been detected with higher resolution ex vivo imaging. While ex vivo microscopy undeniably provides for acquisition of higher-resolution images than in vivo ophthalmoscopy, continued advancements in in vivo imaging techniques may eventually blur this separation. The use of adaptive optics for example, is capable of obtaining transverse plane resolution that rivals that of ex vivo microscopy and can even differentiate, to some extent, depth stratification.[16]

The versatility of organotypic retinal explant culture provides an opportunity to study several exciting aspects of dynamic dendritic remodeling that are currently beyond the capture of in vivo models. Ongoing work aims to expand the scope of this system by leveraging its particular strengths including high resolution of image acquisition. Dendritic spines play an important role in electrophysiological processing and synapse function, and their dynamics have been assessed in RGCs in developing tissue over short periods of time.[20] Dendritic spine dynamics in adult healthy and diseased RGCs are poorly understood and this model could be used to shed light on this issue. In addition, methods for labeling subcellular structures, such as mitochondria, apoptotic machinery, cytoskeletal components, trafficking machinery, and synapses may provide a role for this model in assessing how these structures behave over days in degenerating RGCs. By demonstrating the ability to image RGC structure over the relatively long course of days in retinal organ culture, we hope to expand the scope of inquiry regarding cellular and subcellular processes in the context of RGC degeneration.

Several limitations to the present system deserve attention. The present study limited imaging of RGCs to two time points. Our preliminary data suggest that frequent imaging of RGCs leads to decreased YFP signal intensity, possibly as a result of photobleaching that exceeds the fluorphore production rate (data not shown). It is unclear whether laser scanning confocal microscopy itself induces photoxic effects in the RGCs as a result of the imaging process. While this can be experimentally controlled for, it may potentially add a further layer of RGC stress to the organotypic culture model. Indeed, the applicability of this model to studying human disease such as glaucoma is limited by the fact that explantation requires complete axotomy of the cells being studied.

The injury induced by mechanical axonal injury induces much more rapid and pronounced degenerative changes in RGCs, including within the dendritic tree, than ocular hypertension. The relative merits of direct axonal trauma (crush or axotomy) in modeling glaucoma have been discussed elsewhere,[44] but it is important to consider that glaucomatous optic neuropathy involves a complex, as of yet incompletely understood pathogenesis of RGC injury. Therefore, pathophysiological processes identified in this culture model would need to be validated using in vivo models that better recapitulate certain aspects of the disease. It is interesting and reassuring that the changes we observed with regard to RGC dendrite degeneration in many ways parallel what has been observed using in vivo optic nerve crush models; however, this is measurably different from changes in RGC dendrites detected following experimental IOP elevation.[22]

Another limitation of the current system involves depth of resolution. While confocal microscopy provides for excellent resolution within the transverse plane, the imaging of live tissue necessitates time- and energy-limited imaging protocols that preclude adequate depth resolution to discern sublaminar dendrite projections within the inner plexiform layer. Imaging

Investigative Ophthalmology & Visual Science

of fixed tissue, on the other hand, typically employs high laser power with minimal aperture and image window step size to maximize resolution in the axial plane. This is important missing information as the depth of dendrite projection into target retinal sublamina is necessary to fully subclassify RGGs. It is possible that live-imaging of retinal explants using two-photon microscopy would allow greater resolution in the Z-plane and a greater number of single-plane scans with less phototoxicity, which could provide greater detailed information about sublaminar dendritic projections. It may also allow for more frequent repeated imaging of individual RGCs, thereby increasing the number of time points in longitudinal experiments. This is a subject of ongoing research.

Accurate RGC subclassification is likely to be important in glaucoma where susceptibility to cell death appears to be correlated, at least to some extent, with RGC subtype.[45] Whereas we previously demonstrated that optic nerve crush induces a global degeneration of RGC dendritic trees, IOP elevation by microbead occlusion of the anterior chamber does not appear to trigger dendrite loss on a global RGC population level.[22] However, Della Santina et al.,[46] demonstrated, using the same model, RGC subclass-specific reductions in dendritic field size and complexity that are measurable in cells imaged microscopically post mortem as early as 30 days after induction of ocular hypertension, with OFF-transient RGCs being most clearly affected. El-Danaf and Huberman[41] used the same model to show that degenerative changes to the dendritic tree are observable as early as 7 days post IOP induction, and corroborating the above findings, RGC dendrites that morphologically project to the "OFF" sublamina of the inner plexiform layer as opposed to the "ON" sublamina (regardless of functional "on" or "off" electrophysiological behavior) are most severely affected. Such findings suggest that further enhancements to the current methodology, which would allow for greater depth of field resolution of the dendritic tree for RGCs imaged in time-lapse fashion, may be capable of elucidating more nuanced patterns of dendrite degeneration based on subclass discrimination.

While the present system improves experimental efficiency by reducing the number of RGCs needed for imaging, owing to the fact that paired comparisons provide for more powerful statistical analyses, it should be noted that significantly more RGCs need to be imaged at baseline than will survive to 7 days due to the natural history of RGC death in this model. In the present study, we observed an overall survival rate of approximately 60% at 7 days. We were unable to detect any baseline morphologic characteristics that discriminate those cells likely to remain viable at 7 days. However, imaging cells at more frequent time points and combining the present model with molecular analyses of RGC subgroups may uncover ways of identifying cells more likely to die early following insult. If possible, these cells would be a preferable target for neuroprotective intervention.

The present study demonstrates the use of organotypic retinal explant culture for monitoring complex RGC structure over time in individual cells during the degeneration process. Further experimental usage of this model may be useful for identifying the molecular pathways underlying dendritic pruning in RGC degeneration and for assessing whether purported "neuroprotective" therapies for glaucoma are capable of adequately preventing RGC dendrite degradation, as evidenced by the proof-of-concept shown here that BDNF and CNTF treatment significantly attenuated dendrite degeneration. Continued refinements may provide methods for increasing the frequency of imaging over time and increasing the resolution of imaging for discrimination of subcellular processes taking place within dendrites themselves. The current study adds a potentially useful tool to the experimental repertoire of glaucoma and neuroscience research.

Acknowledgments

Supported by a National Institutes of Health Core Grant EY-O1765 (Bethesda, MD, USA).

Disclosure: **T.V. Johnson**, None; **E.N. Oglesby**, None; **M.R. Steinhart**, None; **E. Cone-Kimball**, None; **J. Jefferys**, None; **H.A. Quigley**, None

References

1. Almasieh M, Wilson AM, Morquette B, Cueva Vargas JL, Di Polo A. The molecular basis of retinal ganglion cell death in glaucoma. *Prog Retin Eye Res*. 2012;31:152–181.
2. Chang EE, Goldberg JL. Glaucoma 2.0: neuroprotection, neuroregeneration, neuroenhancement. *Ophthalmology*. 2012;119:979–986.
3. Tsai JC. Canadian journal of ophthalmology lecture: translational research advances in glaucoma neuroprotection. *Can J Ophthalmol*. 2013;48:141–145.
4. Tezel G. Immune regulation toward immunomodulation for neuroprotection in glaucoma. *Curr Opin Pharmacol*. 2013;13:23–31.
5. Johnson TV, Martin KR. Cell transplantation approaches to retinal ganglion cell neuroprotection in glaucoma. *Curr Opin Pharmacol*. 2013;13:78–82.
6. Morquette JB, Di Polo A. Dendritic and synaptic protection: is it enough to save the retinal ganglion cell body and axon? *J Neuroophthalmol*. 2008;28:144–154.
7. Johnson TV, Bull ND, Martin KR. Stem cell therapy for glaucoma: possibilities and practicalities. *Expert Rev Ophthalmol*. 2011;6:165–174.
8. Karl MO. The potential of stem cell research for the treatment of neuronal damage in glaucoma. *Cell Tissue Res*. 2013;353:311–325.
9. Quigley HA, Addicks EM, Green WR, Maumenee AE. Optic nerve damage in human glaucoma. II. The site of injury and susceptibility to damage. *Arch Ophthalmol*. 1981;99:635–649.
10. Quigley HA, Hohman RM, Addicks EM, Massof RW, Green WR. Morphologic changes in the lamina cribrosa correlated with neural loss in open-angle glaucoma. *Am J Ophthalmol*. 1983;95:673–691.
11. Bellezza AJ, Rintalan CJ, Thompson HW, Downs JC, Hart RT, Burgoyne CF. Deformation of the lamina cribrosa and anterior scleral canal wall in early experimental glaucoma. *Invest Ophthalmol Vis Sci*. 2003;44:623–637.
12. Beirowski B, Babetto E, Coleman MP, Martin KR. The *Wld*^{s} gene delays axonal but not somatic degeneration in a rat glaucoma model. *Eur J Neurosci*. 2008;28:1166–1179.
13. Fernandes KA, Harder JM, John SW, Shrager P, Libby RT. Dlk-dependent signaling is important for somal but not axonal degeneration of retinal ganglion cells following axonal injury. *Neurobiol Dis*. 2014;69:108–116.
14. Yu DY, Cringle SJ, Balaratnasingam C, Morgan WH, Yu PK, Su EN. Retinal ganglion cells: energetics, compartmentation, axonal transport, cytoskeletons and vulnerability. *Prog Retin Eye Res*. 2013;36:217–246.
15. Stevens B, Allen NJ, Vazquez LE, et al. The classical complement cascade mediates CNS synapse elimination. *Cell*. 2007;131:1164–1178.
16. Geng Y, Dubra A, Yin L, et al. Adaptive optics retinal imaging in the living mouse eye. *Biomed Opt Express*. 2012;3:715–734.
17. Lindsey JD, Duong-Polk KX, Hammond D, Chindasub P, Leung CK, Weinreb RN. Differential protection of injured retinal

ganglion cell dendrites by brimonidine. *Invest Ophthalmol Vis Sci*. 2015;56:1789–1804.

18. Walsh MK, Quigley HA. In vivo time-lapse fluorescence imaging of individual retinal ganglion cells in mice. *J Neurosci Methods*. 2008;169:214–221.
19. Leung CK, Weinreb RN, Li ZW, et al. Long-term in vivo imaging and measurement of dendritic shrinkage of retinal ganglion cells. *Invest Ophthalmol Vis Sci*. 2011;52:1539–1547.
20. Xu HP, Chen H, Ding Q, et al. The immune protein CD3zeta is required for normal development of neural circuits in the retina. *Neuron*. 2010;65:503–515.
21. White AJ, Heller JP, Leung J, Tassoni A, Martin KR. Retinal ganglion cell neuroprotection by an angiotensin II blocker in an ex vivo retinal explant model. *J Renin Angiotensin Aldosterone Syst*. 2015;16:1193–1201.
22. Kalesnykas G, Oglesby EN, Zack DJ, et al. Retinal ganglion cell morphology after optic nerve crush and experimental glaucoma. *Invest Ophthalmol Vis Sci*. 2012;53:3847–3857.
23. Liu M, Guo L, Salt TE, Cordeiro MF. Dendritic changes in rat visual pathway associated with experimental ocular hypertension. *Curr Eye Res*. 2014;39:953–963.
24. Morquette B, Morquette P, Agostinone J, et al. Redd2-mediated inhibition of mTOR promotes dendrite retraction induced by axonal injury. *Cell Death Differ*. 2015;22:612–625.
25. Williams PA, Howell GR, Barbay JM, et al. Retinal ganglion cell dendritic atrophy in DBA/2J glaucoma. *PLoS One*. 2013;8: e72282.
26. Tribble JR, Cross SD, Samsel PA, Sengpiel F, Morgan JE. A novel system for the classification of diseased retinal ganglion cells. *Vis Neurosci*. 2014;31:373–380.
27. Feng G, Mellor RH, Bernstein M, et al. Imaging neuronal subsets in transgenic mice expressing multiple spectral variants of GFP. *Neuron*. 2000;28:41–51.
28. Johnson TV, Martin KR. Development and characterization of an adult retinal explant organotypic tissue culture system as an in vitro intraocular stem cell transplantation model. *Invest Ophthalmol Vis Sci*. 2008;49:3503–3512.
29. Bull ND, Johnson TV, Welsapar G, DeKorver NW, Tomarev SI, Martin KR. Use of an adult rat retinal explant model for screening of potential retinal ganglion cell neuroprotective therapies. *Invest Ophthalmol Vis Sci*. 2011;52:3309–3320.
30. Johnson TV, DeKorver NW, Levasseur VA, et al. Identification of retinal ganglion cell neuroprotection conferred by platelet-derived growth factor through analysis of the mesenchymal stem cell secretome. *Brain*. 2014;137:503–519.
31. Meijering E, Jacob M, Sarria JC, Steiner P, Hirling H, Unser M. Design and validation of a tool for neurite tracing and analysis in fluorescence microscopy images. *Cytometry A*. 2004;58: 167–176.
32. Schindelin J, Arganda-Carreras I, Frise E, et al. Fiji: an open-source platform for biological-image analysis. *Nat Methods*. 2012;9:676–682.
33. Kielczewski JL, Pease ME, Quigley HA. The effect of experimental glaucoma and optic nerve transection on amacrine cells in the rat retina. *Invest Ophthalmol Vis Sci*. 2005;46:3188–3196.
34. Duan X, Qiao M, Bei F, Kim IJ, He Z, Sanes JR. Subtype-specific regeneration of retinal ganglion cells following axotomy: effects of osteopontin and mTOR signaling. *Neuron*. 2015; 85:1244–1256.
35. Weber AJ, Harman CD. BDNF preserves the dendritic morphology of alpha and beta ganglion cells in the cat retina after optic nerve injury. *Invest Ophthalmol Vis Sci*. 2008;49: 2456–2463.
36. Drummond ES, Rodger J, Penrose M, Robertson D, Hu Y, Harvey AR. Effects of intravitreal injection of a RHO-GTPase inhibitor (BA-210), or CNTF combined with an analogue of cAMP, on the dendritic morphology of regenerating retinal ganglion cells. *Restor Neurol Neurosci*. 2014;32:391–402.
37. Smith PD, Sun F, Park KK, et al. SOCS3 deletion promotes optic nerve regeneration in vivo. *Neuron*. 2009;64:617–623.
38. Qin S, Zou Y, Zhang CL. Cross-talk between KLF4 and STAT3 regulates axon regeneration. *Nat Commun*. 2013;4:2633.
39. Howell GR, Macalinao DG, Sousa GL, et al. Molecular clustering identifies complement and endothelin induction as early events in a mouse model of glaucoma. *J Clin Invest*. 2011;121:1429–1444.
40. Guo Y, Cepurna WO, Dyck JA, Doser TA, Johnson EC, Morrison JC. Retinal cell responses to elevated intraocular pressure: a gene array comparison between the whole retina and retinal ganglion cell layer. *Invest Ophthalmol Vis Sci*. 2010;51:3003–3018.
41. El-Danaf RN, Huberman AD. Characteristic patterns of dendritic remodeling in early-stage glaucoma: evidence from genetically identified retinal ganglion cell types. *J Neurosci*. 2015;35:2329–2343.
42. Gan WB, Grutzendler J, Wong RO, Lichtman JW. Ballistic delivery of dyes for structural and functional studies of the nervous system. *Cold Spring Harb Protoc*. 2009;2009:pdb prot5202.
43. Stradleigh TW, Greenberg KP, Partida GJ, Pham A, Ishida AT. Moniliform deformation of retinal ganglion cells by formaldehyde-based fixatives. *J Comp Neurol*. 2015;523:545–564.
44. Johnson TV, Tomarev SI. Rodent models of glaucoma. *Brain Res Bull*. 2010;81:349–358.
45. Shou T, Liu J, Wang W, Zhou Y, Zhao K. Differential dendritic shrinkage of alpha and beta retinal ganglion cells in cats with chronic glaucoma. *Invest Ophthalmol Vis Sci*. 2003;44:3005–3010.
46. Della Santina L, Inman DM, Lupien CB, Horner PJ, Wong RO. Differential progression of structural and functional alterations in distinct retinal ganglion cell types in a mouse model of glaucoma. *J Neurosci*. 2013;33:17444–17457.

Investigative Ophthalmology & Visual Science